

# Supernova Inelastic Neutrino-Nucleus Cross Sections from High-Resolution Electron Scattering Experiments and Shell-Model Calculations

K. Langanke,<sup>1</sup> G. Martínez-Pinedo,<sup>2</sup> P. von Neumann-Cosel,<sup>3</sup> and A. Richter<sup>3</sup>

<sup>1</sup>*Institute for Physics and Astronomy, University of Århus, DK-8000 Århus C, Denmark*

<sup>2</sup>*ICREA and Institut d'Estudis Espacials de Catalunya,  
Edifici Nexus, Gran Capità 2, E-08034 Barcelona, Spain*

<sup>3</sup>*Institut für Kernphysik, Technische Universität Darmstadt, 64289 Darmstadt, Germany*

(Dated: November 21, 2018)

Highly precise data on the magnetic dipole strength distributions from the Darmstadt electron linear accelerator for the nuclei  $^{50}\text{Ti}$ ,  $^{52}\text{Cr}$  and  $^{54}\text{Fe}$  are dominated by isovector Gamow-Teller-like contributions and can therefore be translated into inelastic total and differential neutral-current neutrino-nucleus cross sections at supernova neutrino energies. The results agree well with large-scale shell-model calculations, validating this model.

PACS numbers: 21.60.Cs, 25.30.Dh, 27.40.+z, 23.40.-s

Knowledge about inelastic neutrino-nucleus scattering plays an important role in many astrophysical applications, including r-process nucleosynthesis, the synthesis of certain elements like  $^{10,11}\text{B}$  and  $^{19}\text{F}$  during a supernova explosion by the  $\nu$ -process or for the detection of supernova neutrinos (e.g. see [1]). Although inelastic neutrino-nucleus scattering is not yet considered in supernova simulations, several model studies have indicated that it might be relevant to several aspects of supernova physics *i*) for the neutrino opacities and thermalization during the collapse phase, [2]; *ii*) for the revival of the stalled shock in the delayed explosion mechanism [3, 4] and *iii*) for explosive nucleosynthesis [5]. To predict the outcome of supernova simulations with confidence a better handle on neutrino-nucleus interactions is called for [4], in particular on nuclei in the iron mass range  $A \sim 56$  [5]. While charged-current neutrino-nucleus reactions – the inverse of electron and positron captures – are included in supernova simulations [6], inelastic neutrino-nucleus scattering is not. Unfortunately no data for inelastic neutrino-nucleus scattering is currently available (except for the ground state transition to the  $T = 1$  state at 15.11 MeV excitation energy in  $^{12}\text{C}$  [7, 8]). To measure some relevant neutrino-nucleus cross sections (mainly in the iron mass range) a dedicated detector at the Oak Ridge spallation neutron source has been proposed [1]. To sharpen the experimental program at this facility and to improve supernova simulations, inelastic neutrino-nucleus cross sections should be incorporated into the supernova models. It appears as if the needed inelastic neutrino cross sections for iron-region nuclei have to be evaluated by theoretical models without constraint by data. This manuscript will demonstrate that this is in fact not the case. Our aim is to show that precision data on the magnetic dipole ( $M1$ ) strength distributions, obtained by inelastic electron scattering, supply to a large extent the required information about the nuclear Gamow-Teller ( $GT$ ) distribution which determines the inelastic neutrino-nucleus cross sections for

supernova neutrino energies. This intimate relation of  $M1$  and  $GT$  strength has already been exploited before to estimate neutrino cross sections for either individual transitions (e.g. in  $^{12}\text{C}$  [9, 10]) or total cross sections (e.g. in  $^{208}\text{Pb}$  [11, 12]). We will add to this by demonstrating that large-scale shell-model calculations agree quite well with the precision  $M1$  data, thus validating the use of such models to determine the required cross sections for nuclei where no data exist, or at the finite-temperature conditions in a supernova.

The  $M1$  response is one of the fundamental low-energy excitations of the nucleus. It can be well explored by means of inelastic electron scattering. Such transitions are mediated by the operator

$$\mathcal{O}(M1) = \sqrt{\frac{3}{4\pi}} \sum_k [g_l(k)\mathbf{l}(k) + g_s(k)\mathbf{s}(k)]\mu_N \quad (1)$$

where  $\mathbf{l}$  and  $\mathbf{s}$  are the orbital and spin angular momentum operators, and the sum runs over all nucleons. The orbital and spin gyromagnetic factors are given by  $g_l = 1$ ,  $g_s = 5.586$  for protons and  $g_l = 0$ ,  $g_s = -3.826$  for neutrons [13];  $\mu_N$  is the nuclear magneton. Using isospin quantum numbers  $\pm 1/2$  for protons and neutrons, respectively, and  $\mathbf{t}_0 = \boldsymbol{\tau}_0/2$ ; Eq. (1) can be rewritten in isovector and isoscalar parts. Due to a strong cancellation of the  $g$ -factors in the isoscalar part, the isovector part dominates. The respective isovector  $M1$  operator is given by

$$\mathcal{O}(M1)_{\text{iv}} = \sqrt{\frac{3}{4\pi}} \sum_k [\mathbf{l}(k)\mathbf{t}_0(k) + (g_s^p - g_s^n)\mathbf{s}(k)\mathbf{t}_0(k)]\mu_N. \quad (2)$$

We note that the spin part of the isovector  $M1$  operator is the zero component of the  $GT$  operator,

$$\mathcal{O}(GT_0) = \sum_k \boldsymbol{\sigma}(k)\mathbf{t}_0(k) = \sum_k 2\mathbf{s}(k)\mathbf{t}_0(k), \quad (3)$$

however, enhanced by the factor  $\sqrt{3/4\pi}(g_s^p - g_s^n)\mu_N/2 = 2.2993\mu_N$ . On the other hand, inelastic neutrino-nucleus

scattering at low energies, where finite momentum transfer corrections can be neglected, is dominated by allowed transitions. The cross section for a transition from an initial nuclear state ( $i$ ) to a final state ( $f$ ) is given by [10]

$$\sigma_{i,f}(E_\nu) = \frac{G_F^2 g_A^2}{\pi(2J_i + 1)} (E_\nu - \omega)^2 |\langle f || \sum_k \boldsymbol{\sigma}(k) \mathbf{t}(k) || i \rangle|^2, \quad (4)$$

where  $G_F$  and  $g_A$  are the Fermi and axialvector coupling constants, respectively,  $E_\nu$  is the energy of the scattered neutrino and  $\omega$  is the difference between final and initial nuclear energies. Note that for ground state transitions  $E_x = \omega$ . The nuclear dependence is contained in the  $B(GT_0) = g_A^2 |\langle f || \sum_k \boldsymbol{\sigma}(k) \mathbf{t}(k) || i \rangle|^2 / (2J_i + 1)$  reduced transition probability between the initial and final nuclear states.

Thus, experimental  $M1$  data yield the desired  $GT_0$  information, required to determine inelastic neutrino scattering on nuclei at supernova energies, to the extent that the isoscalar and orbital pieces present in the  $M1$  operator can be neglected. On general grounds one expects that the isovector component dominates over the isoscalar piece. Furthermore, it is well known that the major strength of the orbital and spin  $M1$  responses are energetically well separated in the nucleus. In  $pf$ -shell nuclei, which are of interest for supernova neutrino-nucleus scattering, the orbital strength is located at excitation energies  $E_x \simeq 2$ –4 MeV [14], while the spin  $M1$  strength is concentrated between 7 and 11 MeV. A separation of spin and orbital pieces is further facilitated by the fact that the orbital part is strongly related to nuclear deformation [15]. For example, the scissors mode [16], which is the collective orbital  $M1$  excitation, has been detected in well-deformed nuclei like  $^{56}\text{Fe}$  [17]. Thus one can expect that in spherical nuclei the orbital  $M1$  response is not only energetically well separated from the spin part, but also strongly suppressed.

Examples of spherical  $pf$ -shell nuclei are  $^{50}\text{Ti}$ ,  $^{52}\text{Cr}$  and  $^{54}\text{Fe}$ . As these nuclei have also the advantage that precise  $M1$  response data exist from high-resolution inelastic electron scattering experiments [18] we have chosen these 3 nuclei for our further investigation. Our strategy now is to show, in a detailed comparison of data and shell model calculations, that the  $M1$  data indeed represent the desired  $GT_0$  information in a sufficient approximation to transform them into total and differential neutrino-nucleus cross sections. All the total strengths and the strength functions of  $^{50}\text{Ti}$  have been computed using the code NATHAN [19], and the KB3G residual interaction [20] in the complete  $pf$  model space (orbits  $f_{7/2}$ ,  $p_{3/2}$ ,  $p_{1/2}$ , and  $f_{5/2}$ ). For  $^{52}\text{Cr}$  and  $^{54}\text{Fe}$  the strength functions are computed in truncated model spaces, allowing up to 6 and 5 protons and neutrons to be promoted from the lowest  $f_{7/2}$  orbital into the other  $pf$ -shell orbitals, respectively. The  $M1$  and  $GT_0$  response functions are calculated with 400 Lanczos iterations for both

isospin channels. As customary in shell-model calculations, the spin operator is replaced by an effective operator  $\mathbf{s}_{\text{eff}} = 0.75\mathbf{s}$ , where the constant is universal for all  $pf$ -shell nuclei [21].

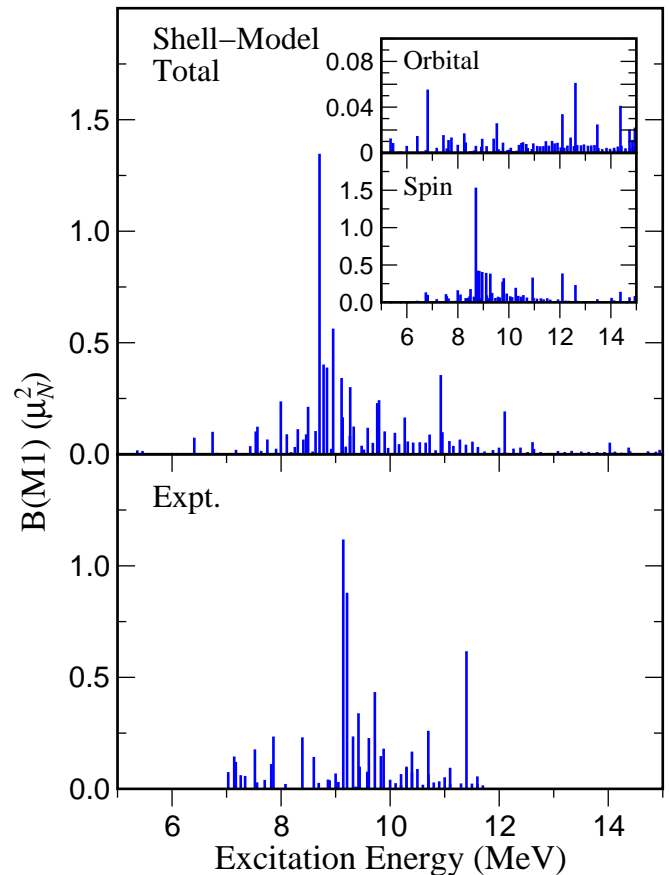


FIG. 1: Comparison of experimental  $M1$  strength distribution [ $B(M1) = |\langle f || \mathbf{O}(M1) || i \rangle|^2 / (2J_i + 1)$ ] in  $^{52}\text{Cr}$  (bottom) with the shell-model result (top). The inset shows the decomposition into spin (bottom) and orbital (top) parts. Note the different scales of the ordinate for the spin and orbital pieces, respectively.

Experimentally  $M1$  data have been determined for the energy intervals 8.5–11.6 MeV in  $^{50}\text{Ti}$  (resolving the  $M1$  strength for 29 individual states), while for the other two nuclei  $M1$  data exist for the energy interval 7.0–11.8 MeV resolving 53 states for  $^{52}\text{Cr}$  and 33 states for  $^{54}\text{Fe}$ . The summed experimental  $B(M1)$  strength (in  $\mu_N^2$ ) in these intervals is 4.5(5) for  $^{50}\text{Ti}$ , 8.1(5) for  $^{52}\text{Cr}$  and 6.6(4) for  $^{54}\text{Fe}$ , which for  $^{50}\text{Ti}$  and  $^{52}\text{Cr}$ , is in agreement with the shell model (4.3 and 7.6, respectively, in the same intervals). For  $^{54}\text{Fe}$  the shell model strength is slightly larger (8.6) than the data, which is also true, if another interaction (GXPF1 [22]) is used (8.4). The total shell model  $B(M1)$  strengths of 7.2 for  $^{50}\text{Ti}$ , 8.7 for  $^{52}\text{Cr}$  and 10.2 for  $^{54}\text{Fe}$  indicate some additional strength outside of the experimental energy window. For a comparison of the  $M1$  strength distributions a problem arises due to uncertain-

ties of the distinction between  $M1$  and  $M2$  transitions in some of the  $(e, e')$  data. Therefore, all possible  $M1$  candidates are modified by the weighing factors introduced in [18] to express the level of confidence of the assignment. The experimental sensitivity limit  $B(M1) \simeq 0.04\mu_N^2$  is also taken into account for comparison with the model results. It should be noted that, where data are available [23, 24] good agreement with nuclear resonance fluorescence experiments is observed for the prominent  $M1$  transitions. This is also the case for other  $pf$ -shell nuclei [25, 26]. For all nuclei, the energy dependence of the observed  $M1$  strength distribution is well reproduced. This is shown in Fig. 1 for the example of  $^{52}\text{Cr}$ .

To determine how well the  $M1$  data might reflect the desired  $GT_0$  information we have performed shell-model calculations for the individual orbital and spin parts of the  $M1$  operator as well as calculations for the  $GT_0$  operator, which, except for a constant factor, represents the isovector spin contribution to the  $M1$  operator. The results are displayed in Fig. 1. As expected for spherical nuclei, the orbital  $M1$  strength is significantly smaller, by about an order of magnitude, than the spin  $M1$  strength. The interference between the orbital and spin parts is state-dependent and is largely cancelled out, when the strength is averaged over several states. A similar situation occurs for the isoscalar spin contribution, but now its contribution to the total strength is even smaller.

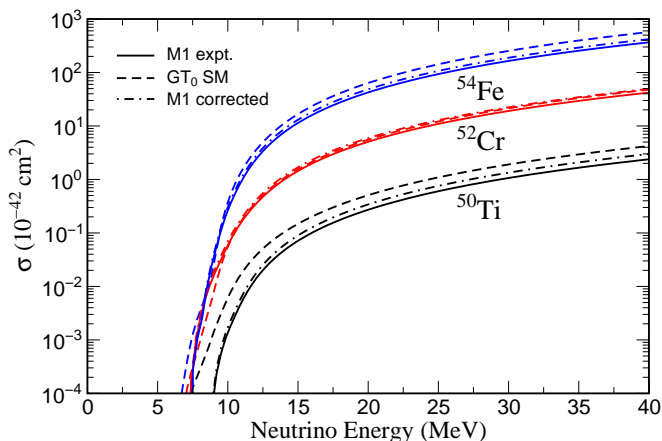


FIG. 2: Neutrino-nucleus cross sections, calculated from the  $M1$  data (solid lines) and the shell-model  $GT_0$  distributions (dotted) for  $^{50}\text{Ti}$  (multiplied by 0.1),  $^{52}\text{Cr}$ , and  $^{54}\text{Fe}$  (times 10). The long-dashed lines show the cross sections from the  $M1$  data, corrected for possible strength outside the experimental energy window.

Supernova simulations require differential neutrino-nucleus cross sections as functions of initial and final neutrino energies, where neutrinos of different flavors are comprised in energy bins of a few MeV [27, 28, 29], i.e., cross sections are averaged over many final nuclear states. Cancelling most of the interference between orbital and spin contributions, the  $M1$  data should repre-

sent the desired  $GT_0$  information, simply using the relation  $B(M1) = 3(g_s^p - g_s^n)^2 \mu_N^2 / (16g_A^2 \pi) B(GT_0)$ . Figure 2 compares the total neutrino-nucleus cross sections for the 3 nuclei, calculated from the experimental  $M1$  data with those obtained from the shell-model  $GT_0$  distribution. As some of the  $M1$  strength is predicted to reside outside of the currently explored experimental energy window, we have corrected for this by multiplying the “ $M1$  cross section” with the ratio  $B(GT_0)/B(GT_0, \Delta E)$ , where  $\Delta E$  defines the experimental energy interval and the ratio is taken from the shell-model calculations. Based on the above theoretical discussion one can assume that the (energetically complete) “ $M1$  cross section” represents the neutrino-nucleus cross sections quite well.

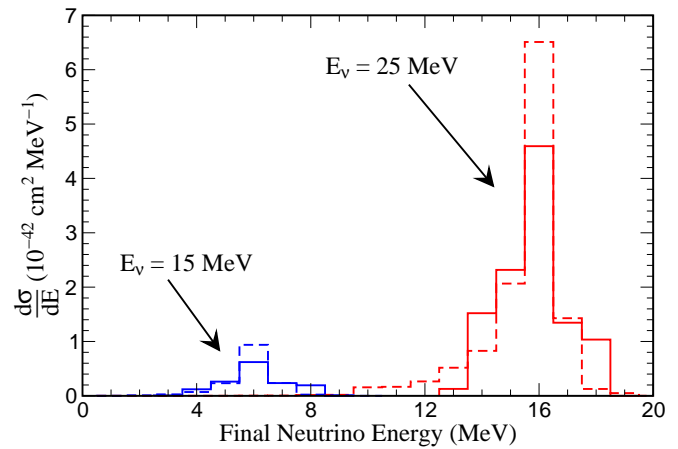


FIG. 3: Differential inelastic neutrino cross sections for  $^{52}\text{Cr}$  and initial neutrino energies  $E_\nu = 15$  MeV and 25 MeV. The solid histograms are obtained from the  $M1$  data, the dashed from shell-model calculations. The final neutrino energies are given by  $E_f = E_\nu - \omega$ .

Figure 3 shows the differential neutrino cross section for  $^{52}\text{Cr}$  at two representative supernova neutrino energies. The cross sections, obtained from the experimental  $M1$  data and the shell model, agree quite well, if binned in energy intervals of a resolution (1 MeV or somewhat larger) as required in supernova simulations.

The comparison of  $M1$  and theoretical cross sections suggests that shell-model based calculations of inelastic neutrino scattering at supernova relevant energies are quite accurate and hence the shell model is the method of choice to determine the cross section for the many nuclei in the iron mass region needed in core-collapse simulations. However, such cross sections require additional considerations so far neglected. These must include the effects of finite momentum transfer, of the finite temperature in the supernova environment and the contributions of additional (forbidden) multipoles to the cross section. The latter become only relevant for neutrino energies which are sufficiently larger than the centroid energy of the respective giant resonance of this multipole. At such neutrino energies the cross section depends only on the

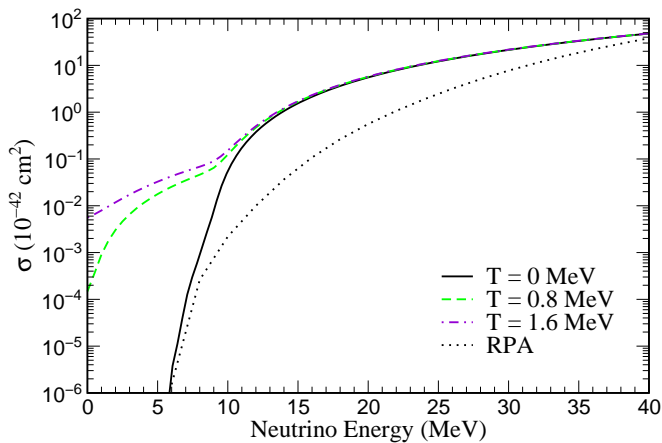


FIG. 4: Inelastic neutrino scattering cross section on  $^{52}\text{Cr}$ , calculated on the basis of shell-model  $GT_0$  distributions at finite temperatures. The dotted curve represents the RPA contributions of other multipoles to the cross sections, including finite-momentum transfer corrections.

total strength of the multipole and its approximate centroid energy (and not on a detailed reproduction of the strength distribution) and is well described within the Random Phase Approximation (RPA) [30]. We have calculated the RPA contribution to the cross section arising from multipoles other than  $GT_0$ , using the formalism of [30, 31] which explicitly considers the finite-momentum dependence of the multipole operators. For the  $GT_0$  component the finite momentum transfer corrections can be considered as described in [32]. Following the approach of [33] we have derived the finite-temperature corrections to the cross sections from the shell model  $GT_0$  transitions between a few hundred excited states and the 6 lowest nuclear states. The  $^{52}\text{Cr}$  cross sections are presented in Fig. 4. Due to the thermal population of excited initial states the neutrino cross sections are significantly enhanced at low energies during the early collapse phase ( $E_\nu \sim 10$  MeV). Once the neutrino energy is large enough to allow scattering to the centroid of the  $GT_0$  strength, which resides at energies around 8–11 MeV, finite temperature effects become unimportant and the neutrino cross section can be derived effectively from the ground state distribution, as discussed in [33], and thus is directly constrained by the  $M1$  data. This applies to the neutrino energy regime relevant to post-shock supernova simulations. Contributions from multipoles other than the  $GT_0$  become important for  $E_\nu > 20$  MeV and dominate for energies higher than 35 MeV.

In summary, we have translated the high-precise ( $e, e'$ )  $M1$  data for  $^{50}\text{Ti}$ ,  $^{52}\text{Cr}$ , and  $^{54}\text{Fe}$ , into detailed total and differential inelastic neutral-current neutrino-nucleus cross sections. Besides representing for the first time detailed neutral-current cross sections for nuclei, such data are in particular important for supernova simulations as they allow to constraint theoretical models needed to

derive the inelastic neutrino-induced cross sections for the many nuclei in the medium-mass range present in a supernova environment. We have further demonstrated that large-scale shell model calculations are able to describe the data, even in details. Following this validation, shell model calculations for inelastic neutrino cross sections on supernova-relevant nuclei are now in progress.

KL is partly supported by the Danish Research Council. GMP is supported by the Spanish MCyT and by the European Union ERDF under contracts AYA2002-04094-C03-02 and AYA2003-06128. PvNC and AR acknowledge support by the DFG under contract SFB 634. Computational cycles were provided by the Centre for Scientific Computing in Århus.

- 
- [1] F. T. Avignone, L. Chatterjee, Y. V. Efremenko, and M. Strayer, eds., *Neutrino physics at spallation neutron sources* (J. Phys. G: Nucl. Part. Phys., 2003), vol. 29, pp. 2497–2676.
  - [2] S. W. Bruenn and W. C. Haxton, *Astrophys. J.* **376**, 678 (1991).
  - [3] W. C. Haxton, *Phys. Rev. Lett.* **60**, 1999 (1988).
  - [4] A. B. Balantekin and G. M. Fuller, *J. Phys. G: Nucl. Part. Phys.* **29**, 2513 (2003).
  - [5] W. R. Hix, A. Mezzacappa, O. E. B. Messer, and S. W. Bruenn, *J. Phys. G: Nucl. Part. Phys.* **29**, 2523 (2003).
  - [6] S. W. Bruenn, *Astrophys. J. Suppl.* **58**, 771 (1985).
  - [7] B. Zeitnitz, *Prog. Part. Nucl. Phys.* **32**, 351 (1994).
  - [8] L. B. Auerbach, et al., *Phys. Rev. C* **64**, 065501 (2001).
  - [9] W. C. Haxton, *Phys. Lett. B* **76**, 165 (1978).
  - [10] T. W. Donnelly and R. P. Peccei, *Phys. Rep.* **50**, 1 (1979).
  - [11] G. M. Fuller, W. C. Haxton, and G. C. McLaughlin, *Phys. Rev. D* **59**, 085005 (1999).
  - [12] N. Jachowicz, K. Heyde, and J. Ryckebusch, *Phys. Rev. C* **66**, 055501 (2002).
  - [13] P. J. Mohr and B. N. Taylor, *Rev. Mod. Phys.* **72**, 351 (2000).
  - [14] T. Guhr, et al., *Z. Phys. A* **336**, 159 (1990).
  - [15] J. Enders, H. Kaiser, P. von Neumann-Cosel, C. Rangacharyulu, and A. Richter, *Phys. Rev. C* **59**, R1851 (1999).
  - [16] D. Bohle, et al., *Phys. Lett. B* **137**, 27 (1984).
  - [17] R. W. Fearick, et al., *Nucl. Phys. A* **727**, 41 (2003).
  - [18] D. I. Sober, et al., *Phys. Rev. C* **31**, 2054 (1985).
  - [19] E. Caurier, et al., *Phys. Rev. C* **59**, 2033 (1999).
  - [20] A. Poves, J. Sánchez-Solano, E. Caurier, and F. Nowacki, *Nucl. Phys. A* **694**, 157 (2001).
  - [21] P. von Neumann-Cosel, A. Poves, J. Retamosa, and A. Richter, *Phys. Lett. B* **443**, 1 (1998).
  - [22] M. Honma, T. Otsuka, B. A. Brown, and T. Mizusaki, *Phys. Rev. C* **69**, 034335 (2004).
  - [23] U. E. P. Berg, et al., *Phys. Lett. B* **103**, 301 (1981).
  - [24] C. Wesselborg, in *Proc. 8th Int. Symp. on Capture Gamma Ray Spectroscopy*, edited by J. Kern (World Scientific, Singapore, 1993), p. 89.
  - [25] A. Degener, et al., *Nucl. Phys. A* **513**, 29 (1990).
  - [26] F. Bauwens, et al., *Phys. Rev. C* **62**, 024302 (2000).
  - [27] M. Liebendörfer, et al., *Astrophys. J. Suppl.* **150**, 263

- (2004).
- [28] M. Rampp and H.-T. Janka, *Astron. & Astrophys.* **396**, 361 (2002).
- [29] A. Burrows, T. Young, P. Pinto, R. Eastman, and T. A. Thompson, *Astrophys. J.* **539**, 865 (2000).
- [30] E. Kolbe, K. Langanke, G. Martínez-Pinedo, and P. Vogel, *J. Phys. G: Nucl. Part. Phys.* **29**, 2569 (2003).
- [31] E. Kolbe, K. Langanke, and P. Vogel, *Nucl. Phys. A* **652**, 91 (1999).
- [32] J. Toivanen, E. Kolbe, K. Langanke, G. Martínez-Pinedo, and P. Vogel, *Nucl. Phys. A* **694**, 395 (2001).
- [33] J. M. Sampaio, K. Langanke, G. Martínez-Pinedo, and D. J. Dean, *Phys. Lett. B* **529**, 19 (2002).